**Interferometer reflection and the right-half-plane zero**
Craig Cahillane
July 2, 2024
Cosmic Explorer DCC T2400008

# 1 Introduction

The Pound-Drever-Hall (PDH) laser frequency error signal is the cornerstone of LIGO. Through it, we achieve extrodinary sensitivity to the round-trip phase $\phi$ accumulated by a laser as it traverses a cavity. The round-trip phase is inaccessible to normal power detection, but by reflecting RF sidebands off the cavity and demodulating at that same RF frequency, we can detect power fluctuations $\delta P_{\mathrm{RF}}$ directly proportional to round-trip phase fluctuations $\delta\phi$.

The phase relationship of the PDH error signal has important implications for control theory as well. Typically, we choose to build *overcoupled* cavities in LIGO, where the input transmission is greater than the end mirror transmission, due to their increased power buildups. Overcoupled cavities exhibit *right-hand-plane zeros* (RHPZ), which help the cavity to lose 360° phase with every free spectral range (FSR). This massive phase loss precludes any kind of basic controller with a bandwidth beyond the FSR. *Undercoupled* cavities, where the input transmission is less than the end mirror transmission, do not suffer from the same phase loss.

As we move forward with Cosmic Explorer, new methods in controlling the main laser frequency must be explored. This may include the possibility of undercoupling the main interferometer, to allow for a high CARM bandwidth beyond the FSR. This would have important implications for the entire lock acquisition process [1–3].

This document overviews the basics of interferometer reflection and coupling, and the impacts on controls. Other nice references on two mirror cavities include [4] and [5].

# 2 Analysis

## 2.1 Fabry-Perot Reflection

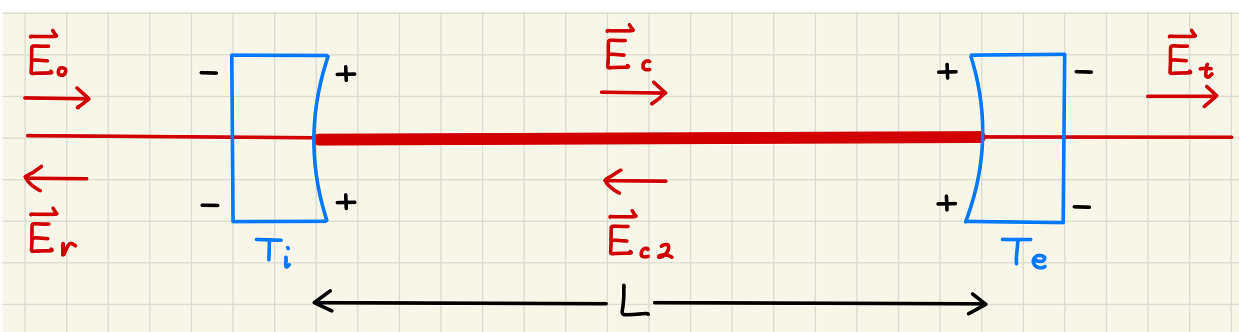


Figure 1: Fabry-Pérot diagram with explicit electric fields.

A two-mirror resonator, or Fabry-Pérot, is shown in Figure 1. The input electric field $E_{\mathrm{in}}$ is incident on the cavity and resonates inside, building up the intracavity field $E_c$. In this diagram,

$T_i$ is the input mirror power transmission,
$R_i = 1 - T_i$ is the input mirror power reflection,
$t_i = \sqrt{T_i}$ is the amplitude transmission,
$r_i = \sqrt{R_i}$ is the amplitude reflection. Similar terms $T_e, R_e, t_e, r_e$ will be used for the end transmission. We assume no losses, so $T_i + R_i = 1$, but losses can be incorporated as a loss in reflectivity without affecting the conclusions here [4].

The plus and minus signs on the mirrors is a convention from the Fresnel relations, where an electric field that reflects off a medium with a lower index of refraction experiences a sign flip. For us, the field reflects off the input mirrors high reflection surface on the inside of the cavity. No phase modification is applied to the transmitted fields.

The Fabry-Pérot reflected field $E_r$ is made up of two superimposed electric fields:
the field transmitting from the resonant $t_i E_{\mathrm{c2}}$,
and the field promptly reflected from the cavity input mirror $-r_i E_{\mathrm{in}}$.

Solving for the reflected field $E_r$ gives you

$$E_r = -r_i E_{\mathrm{in}} + t_i E_{\mathrm{c2}} \tag{1}$$

$$E_r = -r_i E_{\mathrm{in}} + t_i \left( \frac{t_i r_e e^{i\phi}}{1 - r_i r_e e^{i\phi}} \right) E_{\mathrm{in}} \tag{2}$$

$$E_r = \frac{-r_i + (r_i^2 + t_i^2) r_e e^{i\phi}}{1 - r_i r_e e^{i\phi}} E_{\mathrm{in}} \tag{3}$$

where $\phi$ is the round-trip phase of the light in the cavity.

Assuming no losses, Eq. 3 yields the familiar Fabry-Perot reflection transfer function:

$$\frac{E_r}{E_{\mathrm{in}}}(\phi) = \frac{-r_i + r_e e^{i\phi}}{1 - r_i r_e e^{i\phi}} \tag{4}$$

### 2.2 Pound-Drever-Hall Error Signal

The PDH error signal comes from the demodulation of RF sidebands reflected off the cavity [6]. We forego the derivation, of which there are many nice ones, like Appendix C here [7] or Appendix B here [8].

The PDH error signal $S_{\mathrm{PDH}}(\phi)$ has units W/rad and goes like

$$S_{\mathrm{PDH}}(\phi) = \Gamma \left[ E_r(\phi) E_r^*(\phi + \phi_{\mathrm{RF}}) - E_r^*(\phi) E_r(\phi - \phi_{\mathrm{RF}}) \right] \tag{5}$$

We have assumed a RF demodulation and low pass applied to the photodiode signal, as well as a small RF modulation depth $\Gamma$. $\phi_{\mathrm{RF}} = 2\pi f_{\mathrm{RF}}/\mathrm{FSR}$ is the extra phase from the radio-frequency modulation. We will set the RF modulation frequency such that the RF sidebands are not on-resonance, while the carrier is resonant.

The real part of Eq. 5 forms the I-quadruature of the signal which is sensitive to the reflected phase changes. Because the RF sidebands are not on-resonance, for small changes in the round-trip phase $\delta\phi$, $E_r^*(\phi + \phi_{\mathrm{RF}})$ and $E_r(\phi - \phi_{\mathrm{RF}})$ can be treated as constants.

Under these conditions, *the response of the PDH error signal is determined primarily by the carrier reflection response* $E_r(\phi)$. For the rest of this doc, we will consider only the phase dynamics of the reflected signal in Eq. 4.

### 2.3 Coupling Conditions

There are three interferometer coupling conditions, also sometimes called *impedance matching* conditions:

1. *Overcoupled*: $r_i < r_e$
2. *Critically coupled*: $r_i = r_e$
3. *Undercoupled*: $r_i > r_e$

These couplings refer to which term dominates from our early Eq. 1 when on resonance, the promptly reflected field or the transmitted intracavity field.

In the critically coupled case, we have $E_r = 0$ on resonance, meaning that both the intracavity field and promptly reflected field contribute equal and opposite phases to our reflected beam, achieving perfect destructive interference.

In the overcoupled case, as we can see from Eq. 4, we have $E_r > 0$ on resonance. This can be seen most easily in the blue vector in Figure 2. Analyzing Eq. 1, the transmitted intracavity field eliminates the promptly reflected field, leading to a non-zero reflected field dominated by the transmitted intracavity field. Crucially, the transmitted intracavity field accrues the entire round-trip phase of the cavity. This is seen in the reflected signal, causing the $360^\circ$ phase lags seen in Figure 3.

In the undercoupled case, we have $E_r < 0$ on resonance, shown in the green vector in Figure 2. Here, Eq. 1 indicates the promptly reflected field dominates over the transmitted intracavity field for biggest contribution to the reflected field. The promptly reflected field does not accrue the round-trip cavity phase, and does not suffer from the $360^\circ$ phase lags in Figure 3.

Physically, the round-trip phase of the laser light in the cavity $\phi$ is the quantity of interest. The demodulated PDH signal in Eq. 5 picks out the phase information we are interested in. The undercoupled cavity acts as a phase reference to which we can promptly stabilize, without having to wait for new light to resonate and return with the phase information. The difference in phase delay between cavity couplings can be seen in Figure 3.

We note that the sign of the phase change is different between overcoupled and undercoupled systems. Reflected power decreases as we approach resonance, but the change in phase $\delta\phi$ is negative for overcoupled and positive for undercoupled. This impacts the sign of the PDH error signal required to lock. The sign change of the PDH error signal motivates the desire to stay away from the critically coupled lock point, as the zeroing of the PDH error signal will causes locklosses.

For the Figures 2 and 3, we have chosen a low finesse system so the resonance behavior is visible between FSRs. Here, $T_e = 0.5$, and $T_i = 0.55, 0.5, 0.45$ for our overcoupled, critically coupled, and undercoupled systems.

### 2.4 Right-hand-plane zero

A right-hand-plane zero (RHPZ) is a zero in a control loop that has a positive real component in the Laplace-domain, or $s$-domain. One result of a RHPZ is that in the transfer function frequency response, the magnitude starts to rise but the phase starts to fall at the zero's frequency, unlike a typical left-hand-plane zero where the magnitude and phase rise together.

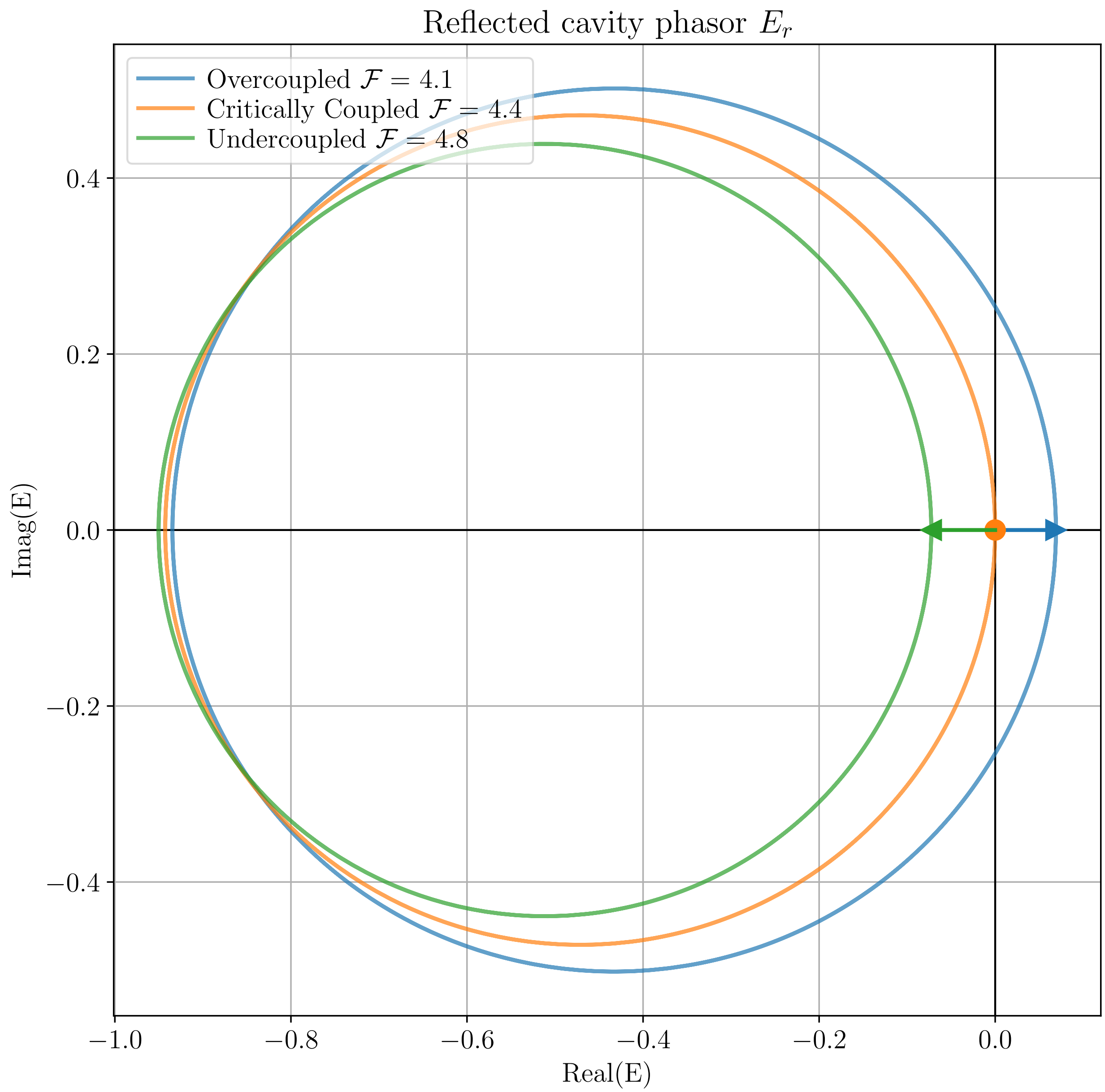


Figure 2: Fabry-Pérot electric field input to reflection phasor. Eq. 4 shows the phasor plotted here. The critically coupled curve occurs when $r_i = r_e$, so when on resonance (i.e. $\phi = 0$), we have $E_r = 0$. The blue and green vectors are drawn for resonance conditions for the overcoupled and undercoupled cavities, respectively.

Recall that right-hand-plane poles (RHPP) will result in a control system that is *unstable*, due to the expontially rising response at the pole frequency. The existance of a RHPZ makes the system *non-minimum phase*. Trying to invert the RHP zero will create a RHP pole and lead to instability. From Eq. 4, we can make some approximations which put it closer to a pole-zero form normally

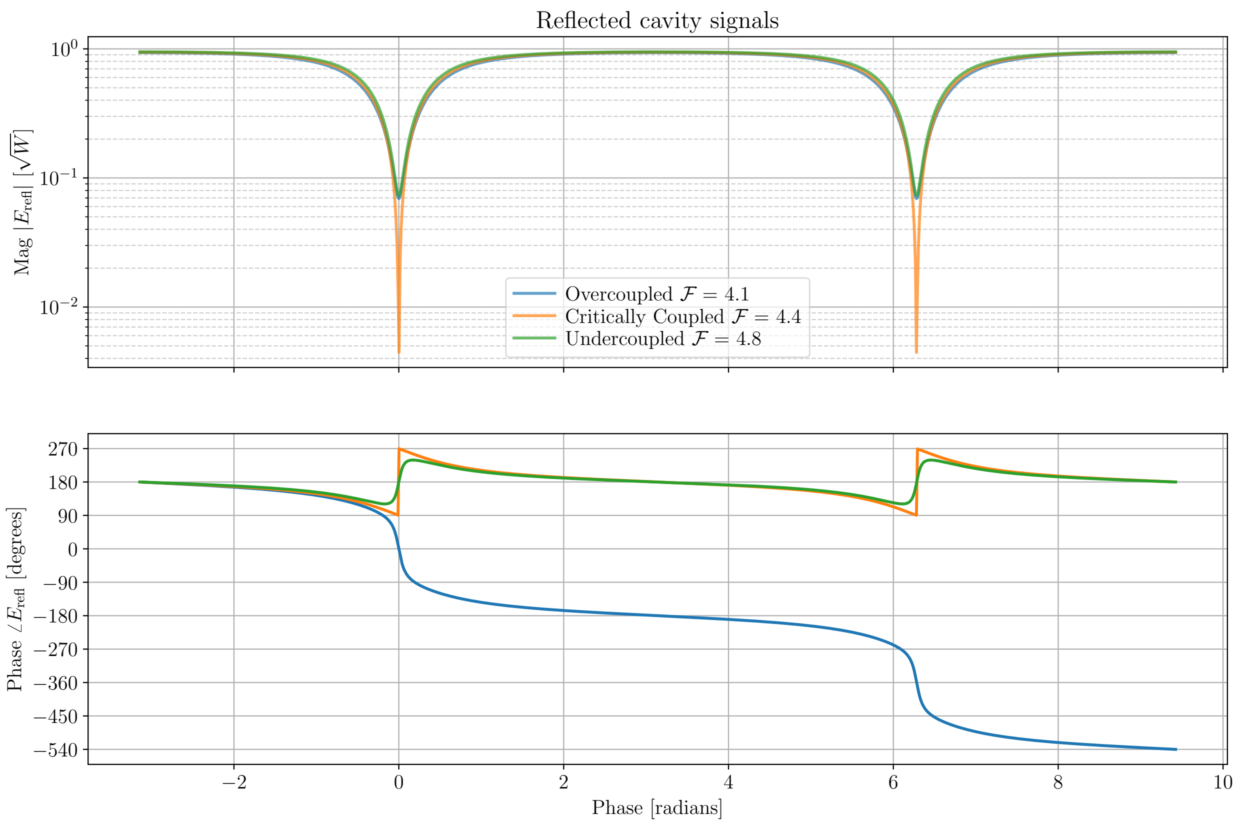


Figure 3: Fabry-Pérot electric field input to reflection transfer function as a function of round-trip phase $\phi$. Eq. 4 shows the transfer function plotted here. The orange critically coupled curve shows the extrodinary phase sensitivity and zero "refl dip" in the magnitude. The blue overcoupled phase curve shows the repeated 360° phase losses at each FSR. The green undercoupled phase curve does not suffer from the same phase loss, as discussed in Section 2.3.

used for control systems.

$$\frac{E_r}{E_{\rm in}} = \frac{-r_i\left(1 - \dfrac{r_e}{r_i} e^{i\phi}\right)}{1 - r_i r_e e^{i\phi}} \tag{6}$$

$$\frac{E_r}{E_{\rm in}} \approx \frac{-r_i\left(1 + i\dfrac{f}{f_z}\right)}{1 + i\dfrac{f}{f_p}} \tag{7}$$

where the zero $f_z$ and pole $f_p$ are

$$f_p = -\frac{\rm FSR}{2\pi}\log\left(\frac{1}{r_i r_e}\right) \tag{8}$$

$$f_z = -\frac{\rm FSR}{2\pi}\log\left(\frac{r_i}{r_e}\right) \tag{9}$$

The zero $f_z$ changes sign between the overcoupled $r_i < r_e$ and undercoupled $r_i > r_e$ case. In the overcoupled case, $f_z$ must be *less than zero*, leading to the right-half-plane zero. In the undercoupled case, $f_z$ must be greater than zero, leading to the generally preferred left-half-plane zero. The pole $f_p$ must always be greater than zero, because $r_i r_e < 1$.

Looking at the transfer functions in Figure 3, we can understand the effect of the phase lags. In any system, in the leadup to the first resonance we see both the pole $f_p$ and the zero $f_z$, with the pole being first. For the undercoupled system, we first lose phase with the pole, then gain the phase back with the zero, yielding zero total phase change directly on resonance. For the overcoupled system, both the left-hand-plane pole and the right-hand-plane zero cause $90^\circ$ phase lags, leading to $180^\circ$ total phase loss directly on resonance.

On the other side of resonance, the opposite happens, with the zero then pole being experienced by the system. This gives us another $180^\circ$ phase lag for overcoupled systems.

In total, one pass through the FSR yields $0^\circ$ phase lag for undercoupled cavities, as the two poles and zeros counteract one another, but $360^\circ$ phase lag for overcoupled cavities, as the left-hand-plane poles and right-hand-plane zeros both work to amplify the phase loss.

For our overcoupled cavity system in Advanced LIGO, this extreme phase lag at the FSR means we *cannot extend the bandwidth of the PDH controller beyond the FSR*. If we did, we would essentially be trying to invert a right-hand-plane zero, leading to a right-hand-plane pole and a runaway exponential response. Another discussion of this phenomenon is found in [5].

## 3 Conclusions

In short, an undercoupled interferometer can achieve a higher bandwidth than an overcoupled one, because the signal comes primarily from the promptly reflected electric field. The undercoupled cavity itself acts as a stationary phase reference. The cost you pay is (perhaps) a lower power recycling gain and a reduced phase sensitivity. Both of these costs could potentially be designed around.

For the actual LIGO interferometer, we have coupled cavities which make the sign of the zero more complex to calculate [9, 10]. However, the control system stability considerations remain similar.

We may launch an investigation into the possibility of undercoupling the Cosmic Explorer interferometer. This could allow a high-bandwidth CARM loop, which could benefit the low-frequency frequency noise suppression, which could pose as a noise limitation for Cosmic Explorer according to [11].

There will be some ramifications on the lock acquisition process and corner control should we choose to undercouple. Other options could include using POP (or some other intracavity pickoff) to lock CARM, or designing a complex control system to lock a high-bandwidth DC CARM loop for $0 < f <$ FSR, hand off CARM control to IMC1 at the FSR, then ramping up another AC CARM loop for control between FSR $< f < 2$ FSR.

## References


[1] M. Evans, N. Mavalvala, et al. “Lock acquisition of a gravitational-wave interferometer”. In: *Opt. Lett.* 27.8 (2002), pp. 598–600. DOI: 10.1364/OL.27.000598. URL: https://opg.optica.org/ol/abstract.cfm?URI=ol-27-8-598.

[2] A. Staley, D. Martynov, et al. "Achieving resonance in the Advanced LIGO gravitational-wave interferometer". In: *Classical and Quantum Gravity* 31.24 (2014), p. 245010. DOI: 10.1088/0264-9381/31/24/245010. URL: https://dx.doi.org/10.1088/0264-9381/31/24/245010.

[3] K. Arai, M. Ando, et al. "New signal extraction scheme with harmonic demodulation for power-recycled Fabry-Perot-Michelson interferometers". In: *Physics Letters A* 273.1 (2000), pp. 15–24. ISSN: 0375-9601. DOI: https://doi.org/10.1016/S0375-9601(00)00467-9. URL: http://www.sciencedirect.com/science/article/pii/S0375960100004679.

[4] T. Isogai, J. Miller, et al. "Loss in long-storage-time optical cavities". In: *Opt. Express* 21.24 (2013), pp. 30114–30125. DOI: 10.1364/OE.21.030114. URL: https://opg.optica.org/oe/abstract.cfm?URI=oe-21-24-30114.

[5] M. Rakhmanov, R. Savage, et al. "Dynamic resonance of light in Fabry-Perot cavities". In: *Physics Letters A* 305.5 (2002), pp. 239–244. ISSN: 0375-9601. DOI: https://doi.org/10.1016/S0375-9601(02)01469-X. URL: https://www.sciencedirect.com/science/article/pii/S037596010201469X.

[6] R. W. Drever, J. L. Hall, et al. "Laser phase and frequency stabilization using an optical resonator". In: *Applied Physics B Photophysics and Laser Chemistry* (1983). ISSN: 14320649. DOI: 10.1007/BF00702605.

[7] E. D. Hall. PhD thesis. California Institute of Technology, 2017. DOI: 10.7907/Z9PG1PQ9. URL: https://thesis.library.caltech.edu/10031/.

[8] J. C. Driggers. "Noise Cancellation for Gravitational Wave Detectors". en. PhD thesis. 2015. DOI: 10.7907/Z94F1NNP. URL: https://resolver.caltech.edu/CaltechTHESIS:06052015-123753277.

[9] D. Sigg. *Frequency Response of the LIGO Interferometer*. Tech. rep. 1997, T970084. URL: https://dcc.ligo.org/LIGO-T970084/public.

[10] K. Izumi and D. Sigg. "Advanced LIGO: length sensing and control in a dual recycled interferometric gravitational wave antenna". In: *Classical and Quantum Gravity* 34.1 (2017), p. 015001. URL: http://iopscience.iop.org/article/10.1088/0264-9381/34/1/015001.

[11] C. Cahillane, G. L. Mansell, et al. "Laser frequency noise in next generation gravitational-wave detectors". In: *Opt. Express* 29.25 (2021), pp. 42144–42161. DOI: 10.1364/OE.439253. URL: https://opg.optica.org/oe/abstract.cfm?URI=oe-29-25-42144.